A MULTI-PHASE HYGRO-THERMAL MODEL FOR WOODEN BRIDGE COMPONENTS EXPOSED TO SOLAR RADIATION

Stefania Fortino[1], Petr Hradil[2], Timo Avikainen[3], Keijo Koski[4], Ludovic Fülöp [5]

ABSTRACT: This study demonstrates the modelling assisted long-term monitoring of wooden bridge components with surfaces exposed to solar radiation. An improved multi-phase finite element model is developed to predict the distribution of moisture content, relative humidity and temperature in wood. Hygro-thermal measurements are collected from the monitoring system of the stress-laminated Tapiola Bridge in Finland. The monitoring uses integrated sensors which provide both the relative humidity and the temperature in given locations of the deck, which are compared to the numerical results. The modelling assisted monitoring can help to reduce the maintenance costs of timber bridges, as well as the cost of instrumentation, and to increase the safety.

KEYWORDS: Wooden bridges, Wood moisture, Solar radiation, Monitoring, Multi-phase models, Finite Element Method

1 INTRODUCTION

Wooden bridges are economical, show an excellent environmental performance and can have a long service life. However, their durability under harsh climates represents one of the main problems for designers and owners. This is due to the material biodegradation caused by moisture content (*MC*) accumulated in wood for long periods, in combination with certain temperatures [1]. Although evidence exists that structural wood can retain its strength through many centuries, the variations of moisture content can strongly influence the structural integrity, the serviceability, and the loading capacity of timber bridges [2].

In this context, the monitoring of moisture content in wood is necessary for both the durability of the material and the performance of the whole structure. In the last decade, several studies have shown that numerical modelling can assist the sensor-based monitoring to get detailed information on the hygro-thermal response of wooden bridge components (see [3] and the related references).

In previous works [2,3], a multi-phase model with separated water phases was found efficient to study the moisture transport in uncoated and coated stress-laminated timber decks below the fibre saturation point (FSP) under outdoor environmental conditions characterized by continuous variations of temperature (*T*) and relative humidity (*RH*).

This paper presents a multi-phase hygro-thermal model able to simulate the effects of the external climate, including the solar radiation, on the sun exposed surfaces of timber bridge decks. As a case-study, the hygro-thermal analysis of the stress-laminated timber deck of Tapiola Bridge in Finland [2] is carried out by using the finite element method (FEM).

2 MULTI-PHASE MODEL FOR MOISTURE TRANSPORT IN WOOD

Below the FSP, the phenomena governing the moisture transport in wood are the diffusion of water vapour in the pores, the sorption of bound water and the diffusion of bound water in the cell walls [4]. Above the FSP, there are capillary pressure and gravity for the free water in the pores, sorption between the free water and the bound water phases, evaporation or condensation between the free water and the vapour water phases [5]. In the differential equations describing the above phenomena, the water phases are separated and the coupling between them is defined through conversion rates.

Compared to the previous works by some of the authors, in the present paper the influence of the solar radiation during time is considered by modifying the hygro-thermal boundary conditions for the temperature.

2.1 Governing equations

By using a matrix and vector notation, and considering as variables of the problem the bound water concentration c_b, the water vapour concentration c_v and the temperature T in the wood material, the related governing equations are defined as

[1] Stefania Fortino, VTT Technical Research Centre of Finland Ltd, Finland, stefania.fortino@vtt.fi
[2] Petr Hradil, VTT Technical Research Centre of Finland Ltd, Finland, petr.hradil@vtt.fi
[3] Timo Avikainen, VTT Technical Research Centre of Finland Ltd, Finland, timo.avikainen@vtt.fi

[4] Keijo Koski, VTT Technical Research Centre of Finland Ltd, Finland, keijo.koski@vtt.fi
[5] Ludovic Fülöp, VTT Technical Research Centre of Finland Ltd, Finland, ludovic.fulop@vtt.fi

$$\frac{\partial c_b}{\partial t} = -\nabla \cdot \mathbf{J}_b + \dot{c}_{bv} \tag{1}$$

$$\frac{\partial c_v}{\partial t} = -\nabla \cdot \mathbf{J}_v - \dot{c}_{bv} \tag{2}$$

$$c_w \varrho \frac{\partial T}{\partial t} = -\nabla \cdot \mathbf{J}_T - \nabla \cdot \mathbf{J}_b h_b - \nabla \cdot \mathbf{J}_v h_v \\ + \dot{c}_{bv} h_{bv} \tag{3}$$

In the above equations, $\mathbf{J}_b$ and $\mathbf{J}_v$ represent the fluxes of bound water and water vapour defined as

$$\mathbf{J}_b = -\mathbf{D}_b \nabla c_b; \quad \mathbf{J}_v = -\mathbf{D}_v \nabla c_v \tag{4}$$

where ∇ is the nabla operator, $\mathbf{D}_b$ and $\mathbf{D}_v$ are the diffusion matrices for bound water and water vapour phases and the thermal flux $\mathbf{J}_T$ is defined as

$$\mathbf{J}_T = -\mathbf{K}\nabla T \tag{5}$$

where $\mathbf{K}$ is the thermal conductivity matrix. Coupled hygro-thermal terms in fluxes of Equation (4) are not included since their effects were found negligible in the presence of Northern weather conditions [6].

In Equations (1-3) $\dot{c}_{bv}$ represents the conversion rate between the bound water and the water vapour phases. In Equation (3), h_b and h_v are the specific enthalpies and $h_{bv} = h_b - h_v$ the specific transition enthalpy from bound water to water vapour.

The bound water concentration is defined as $c_b = \varrho_0 MC$ where MC is the moisture content and ϱ_0 the dry wood density. The water vapour concentration c_v is a function of the partial vapour pressure p_v through the ideal gas law $c_v = \varphi\, p_v M_{H2O}/RT$ where R is the gas constant and M_{H2O} the molecular mass of water. The vapour pressure is expressed as a function of the relative humidity RH:

$$p_v = RH \cdot p_{vs} \tag{6}$$

where p_{vs} is the saturated vapour pressure given by the semi-empirical Kirchhoff expression [4].

The equation describing the conversion rate between bound water and water vapour is defined as

$$\dot{c}_{bv} = H_c(\varrho_0 MC_{bl} - c_b) \tag{7}$$

where H_c is the moisture dependent reaction rate and MC_{bl} represent the temperature dependent sorption isotherms based on the Anderson-McCarthy model:

$$MC_{bl,\alpha} = -\frac{1}{f_{2\alpha}}\ln\left(\frac{\ln\left(\frac{1}{RH}\right)}{f_{1\alpha}}\right), \quad \alpha \in \{a,d\} \tag{8}$$

where a and d refer to adsorption and desorption and $f_{i\alpha} = \sum_{j=0}^{n} b_{ij\alpha} T^j, \ i \in \{1,2\}$.

All material properties of the model equations presented above, as well as the parameters of the Anderson-McCarthy model can be found in [3].

2.2 Hygro-thermal boundary conditions in the presence of solar radiation

The boundary conditions for bound water and water vapour concentrations are defined as:

$$\mathbf{n} \cdot \mathbf{J}_b = 0 ; \quad \mathbf{n} \cdot \mathbf{J}_v = k_v^w c_v' - k_v^a c_v^a \tag{9}$$

where the first equation holds on all the external surfaces considering that the bound water cannot pass them and it is restricted in the cell walls. Therefore the model includes only exchanges of vapour and heat with the ambient air. In the second equation, defined on the surfaces exposed to RH and T, $\mathbf{n}$ represents the outward normal direction to the surface, $c_v' = c_v/\varphi$ is the concentration of water vapour divided by the wood porosity φ, c_v^a is the water vapour concentration of the air, k_v^w and k_v^a represent the surface permeances related to wood temperature and air temperature, respectively.

In the presence of a paint, the permeances of the coated wood referred to wood temperature and air temperature are defined as in [3]:

$$k_v^w = \frac{1}{\frac{1}{k_w} + \frac{1}{k_p}}\frac{RT}{M_{H2O}}, \qquad k_v^a = \frac{1}{\frac{1}{k_w} + \frac{1}{k_p}}\frac{RT^a}{M_{H2O}} \tag{10}$$

where k_w is the permeance of uncoated wood and k_p the one of the paint.

The boundary condition for the temperature is defined as

$$\mathbf{n} \cdot \mathbf{J}_T = k_T(T - T^a) - q_{r,net} \tag{11}$$

where k_T is the thermal emission coefficient, T^a the temperature of the air, and $q_{r,net}$ represents the so-called net radiance at the wood surface [7]:

$$q_{r,net} = \alpha G + \varepsilon L - \varepsilon\sigma T^4 \tag{12}$$

where α is the solar absorptivity, G the incident solar radiation, ε the longwave emissivity of the surface, L the longwave incident radiation, and σ the Stefan-Boltzmann constant.

The values of dimensionless parameters α and ε depend on the wood material and the type of coating. In [7], the values of α for Korean wood species are around 0.3-0.5 and the values of ε around 0.4-0.7. According to [8], the solar absorptivity increases from a minimum of 0.25 for white paints to a maximum of 0.97 for black paints.

Following [8], the equation that relates the incident angle I on a surface with the solar altitude h, the surface solar azimuth A_{SS} and the orientation of the surface E (i.e. the angle of the surface from the horizontal), is the following:

$$Cos(I) = \cos(h)\cos(A_{SS})\sin(E) \\ + \sin(h)\cos(E) \qquad (13)$$

where the solar altitude is a function of the declination angle [9]. Therefore the incident radiation of Equation (12) is multiplied by the $Cos(I)$.

2.2.1 Implementation in Abaqus FEM code

The multi-phase model is implemented in the user subroutine UEL of Abaqus finite element code to describe the three differential equations of the material model and their boundary conditions [3]. At every time increment, the subroutine reads the weather data from the database of measured temperatures, air relative humidities, and solar radiation data. The shape functions for 8-nodes isoparametric brick elements are used to build a finite element with three variables per node (bound water concentration, water vapour concentration and temperature). The time integration is carried out using the fully implicit Euler scheme and the nonlinear system is solved using the Newton method at each time step. The subroutine allows to implement the FEM contributions to the residual vector and to the Jacobian iteration matrix.

3 ANALYSIS OF THE TAPIOLA BRIDGE DECK

The hygro-thermal data in wood are collected from the on-going monitoring of the stress-laminated timber deck of Tapiola Bridge built in the Spring of 2019 in the city of Espoo, Finland (Figure 1).

The Tapiola Bridge is composed of three spans and two of these are stress-laminated timber decks compressed by steel bars in the transverse direction. The bridge deck is composed of 46 timber beams in the width direction. The laminations are 0.215 m wide, and the deck thicknesses are 0.765 m for the 13.45 m span and 1.035 m for the 22.13 m span. The timber decks are 9.89 m wide and are protected with Valtti colour, an oil-based wood stain produced by Tikkurila corporation [10].

Five integrated humidity-temperature sensors, two force sensors and two displacement sensors were installed to monitor the bridge (Figures 3-5). The monitoring unit cabinet is equipped with two thermocouples for tracking its inside and outside temperature. The reader can refer to publication [2] for more details on the bridge structure and the monitoring system.

The parameters used for the boundary conditions of the case-study, are listed in Table 1. For the coated wood, the used parameters consider also the presence of a shading rail on the deck surface.

3.1 Description of the FEM model

The hygro-thermal model proposed in this work is based on the multi-phase moisture transport theory described in Section 2 with the aim to predict the distribution of *MC*, *RH*, and temperature in wood.

Table 1: *Boundary conditions parameters in the presence of solar radiation*

parameter	value	units
k_w	5.0E-9	kg/ m^2 s Pa
k_p	4.0E-9	kg/ m^2 s Pa
k_T	20	W m^{-2} K^{-1}
α (coated wood)	0.35	-
ε (coated wood)	0.5	-
α (asphalt)	0.7	-
ε (asphalt)	1.0	-
Stefan-Boltzmann constant	5.67×10^{-8}	W/m^2 K^4

Figure 1: *View of Tapiola Bridge*
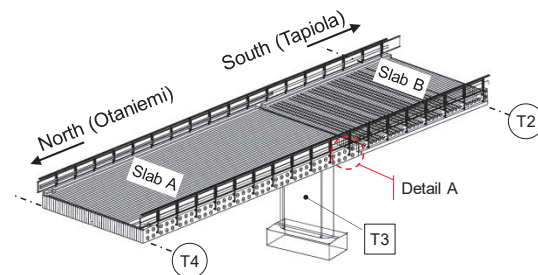
Figure 2: *Scheme of the transverse prestressed glulam wooden slabs of the bridge. The location of the sensors is highlighted as Detail A, in the vicinity of support T3*
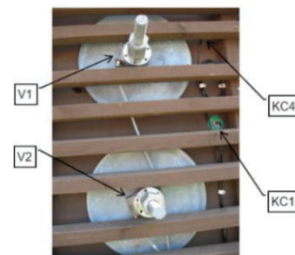
Figure 3: *Photo of the sensor locations. KC1 and KC4: humidity and temperature sensors, V1 and V2: force sensors*
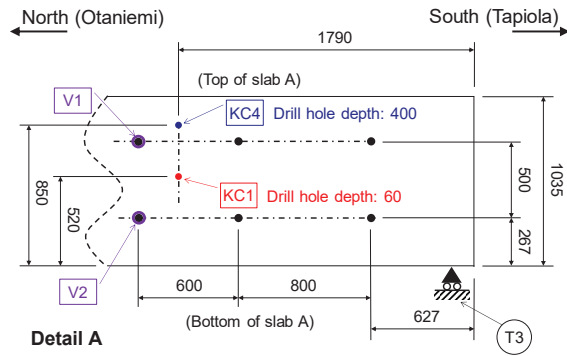
Figure 4: *Sensor locations in the side of the south-west corner of Slab A in the vicinity of support T3*
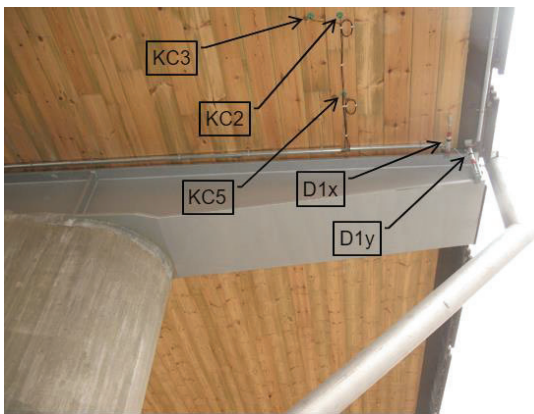
Figure 5: *Photo of the sensor locations on the bottom of the deck. KC2, KC3 and KC5: humidity and temperature sensors, D1x (slab longitudinal displacement) and D1y (slab vertical displacement)*
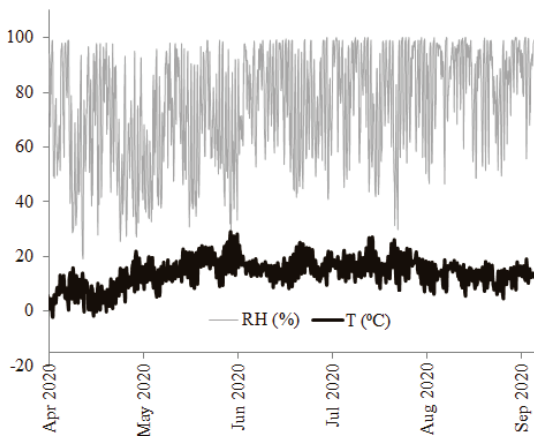
Figure 6: *Hourly relative humidity (RH) and temperature (T) of the air*
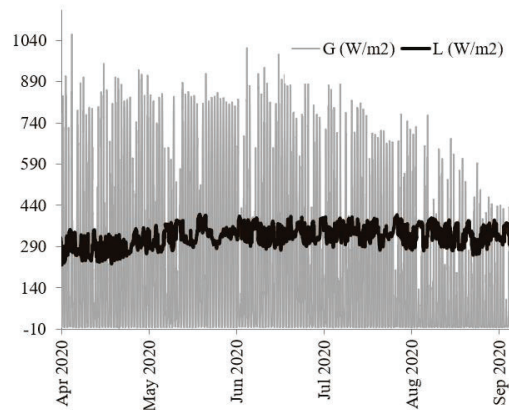
Figure 7: *Hourly incident solar radiation (G) and longwave incident radiation (L) on the exposed surface*

To investigate the hygro-thermal response of the timber deck during the sunny months, characterized by higher temperatures, a six month numerical analysis is carried out from the beginning of April 2020 to the end of September 2020. The hourly air temperature and *RH* are shown in Figure 6, while Figure 7 presents the hourly incident solar radiation and longwave incident radiation. According to the approach proposed in [2], the modelling of the deck for the case-study investigated in this paper is based on the following scheme and assumptions:

- The deck model is schematized as a representative three-dimensional slice having a width of 215 mm (width of the lamination), height 1035 mm (thickness of the deck) and a thickness of 5 mm.
- Since the top surface is protected from moisture by the asphalt layer, it is considered to be exposed only to a thermal flux.
- The asphalt layer is not modelled as material, but higher values of solar absorptivity and longwave emissivity are applied on the top surface of the modelled slice (see Table 1).
- Compared to the model for internal lamination presented in [2], both fluxes of temperature and relative humidity act on the bottom surface as well as on the lateral surface of the lamination exposed to the air. The solar radiation acts on the lateral surface (Figures 3,4).
- The effect of the glue between laminations is not considered.

The used mesh size of the finite element model for the Abaqus analysis is set between 5 and 10 mm.

The solar radiation on the surfaces exposed to the sun affects the whole hygro-thermal response of the analyzed volume of wood because of the temperature increase on the surface. As observed in [8], the temperature of a vertical surface increases faster than for a horizontal surface because the vertical one receives more solar radiation in the early morning. When the sun rises, the incident angle on the vertical surface decreases while the incident angle on a horizontal surface increases. Therefore

452

the temperature of a horizontal surface can reach higher values than a vertical surface. The lateral surface of Tapiola Bridge's deck with sensor KC1 is north-west oriented and receives solar radiation during the afternoon.

3.2   RESULTS AND DISCUSSION

Figures 8 and 9 present the temperatures and the vapor pressures in the wood predicted by the model in the middle height of lamination at a distance of 60 mm from the lateral surface exposed to the afternoon solar radiation. The comparison with the measured temperatures and the vapor pressures in KC1 sensor are in good agreement. This also means that the parameters listed in Table 1 are suitable for the model used in the present case-study. The reported vapor pressure is based on the measured relative humidity. The numerical moisture content in the same location and the *MC* on the surface exposed to the sun are drawn in Figure 10. Table 2 summarizes the maximum and minimum numerical values of moisture contents in the sensor location affected by solar radiation (KC1) and on the sensor location at 60 mm from the bottom of the deck (KC2) previously investigated in [2]. It can be observed that the moisture contents are lower in the presence of solar radiation, and the differences are around 5%. On the exposed surface at the middle height of lamination, the predicted moisture contents in the studied period (Figure 10) are very similar to the ones founded at the bottom surface in a previous study [2]. It should be noticed that the lateral surface of the deck is also exposed to the variable relative humidity and this effect is coupled with the increase of temperature due to the solar radiation.

For future work, it is suggested to simulate cases of untreated wood and wood protected by different coatings to better evaluate the performance of the proposed model. Locations closer to the external surfaces should also be monitored by humidity-temperature sensors for accurate validation of the numerical model. In addition, different climates should be tested, especially in Southern Europe environments.

Developments of coupled hygro-thermal models for timber decks allow the accurate evaluation of moisture contents which is important for the prediction of moisture induced stresses (MIS) by using a sequential mechanical analysis [11]. The MIS can cause surface cracking, cupping deformations and losses of the pre-stress force in steel bars [1]. The accurate prediction of temperature increase due to solar radiation is also important for the investigation of wood decay and resistance of wood in connection with dose models [12].

Table 2: *Maximum and minimum predicted MCs in sensor locations from April 2002 to September 2020*

location	max *MC* (%)	min *MC* (%)
KC1	15.9	15
KC2	16.7	15.8
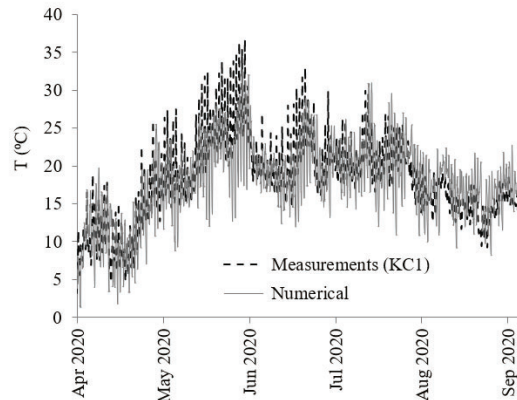
Figure 8: *Measured and predicted temperatures in KC1 sensor location*
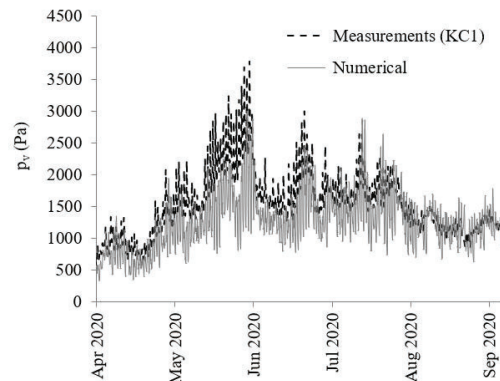
Figure 9: *Measured and predicted vapor pressures in KC1 sensor location*
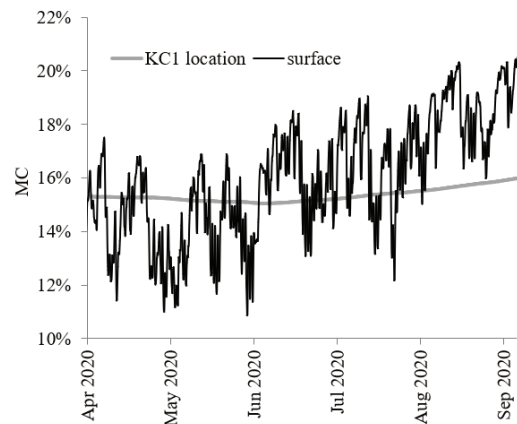
Figure 10: *Predicted moisture contents in KC1 sensor location and on the surface exposed to sun*

In future work, a more general model able to simulate the effects of external climates in wood also in the presence of rain, should consider the free water in lumens above the fibre saturation point [5].

Improved hygro-thermal models, along with sequential mechanical analyses, can reduce the whole costs of timber bridge monitoring and maintenance and increase their safety. The integration of numerical models with sensor-based instrumentation, will indeed reduce the number of needed sensors. In addition, predictions of moisture contents, moisture gradients and the possible crack risk due to the related surface MIS, provide important suggestions for optimal maintenance and eventual repair of the protective system. For instance, it would be practical to check the conditions of paints in certain seasons of the year, as the beginning of summer, characterized by drying in wood.

4 CONCLUSIONS

This paper proposed a multi-phase model for moisture transport able to simulate the hygro-thermal behaviour of a coated wooden bridge deck also considering the effects of solar radiation. The deck is schematized as a three-dimensional slice with the hygro-thermal fluxes on the exposed surfaces and therefore the related FEM analysis is efficient. The results of the model are in good agreement with the monitored data.

To the knowledge of the authors, the effect of solar radiation has not been deeply investigated within multi-phase models with separated water phases previously. Therefore, the proposed model contributes to the scientific advances of this field of research. However, further work is needed to properly validate the model for untreated wood materials and different coatings.

The improved model, used to assist the monitoring, can help to reduce the maintenance costs of timber bridges, as well as the cost of instrumentation, and to increase the safety of these structures.

REFERENCES

[1] Pousette A., Malo K., Thelandersson S., Fortino S., Salokangas L., Wacker J. Durable Timber Bridges - Final Report and Guidelines. SP Report 25. Research Institutes of Sweden RISE, Skellefteå, Sweden, 2017.

[2] Fortino S, Hradil P, Koski K, Korkealaakso A, Fülöp L, Burkart H, Tirkkonen T. Health Monitoring of Stress-Laminated Timber Bridges Assisted by a Hygro-Thermal Model for Wood Material. *Applied Sciences* 11(1):98, 2021.

[3] Fortino S., Hradil P., Genoese A., Genoese A., Pousette A. Numerical hygro-thermal analysis of coated wooden bridge members exposed to Northern European climates. *Construction and Building Materials* 208, 492–505, 2019.

[4] Frandsen, H.L. Selected Constitutive models for simulating the hygromechanical response of wood. Ph.D. Thesis, Dept. of Civil Engineering Aalborg University, Aalborg, Denmark, 2007.

[5] Autengruber M., Lukacevic M., Füssl J. Finite-element-based moisture transport model for wood including free water above the fiber saturation point. *International Journal of Heat and Mass Transfer* 161, 120228:1–120228:21, 2020.

[6] Fortino S. Hradil P., Genoese A., Genoese A., Pousette A., Fjellström P.A. A multi-Fickian hygro-thermal model for timber bridge elements under Northern Europe climates. Proceedings of World conference in Timber Engineering (WCTE 2016) conference, August 22-25.2015, Vienna, Austria.

[7] Kang W., Lee Y-H., Kang C-W., Chung W-Y., Xu H-L., Matsamura J. Using the Inverse Method to Estimate the Solar Absorptivity and Emissivity of Wood Exposed to the Outdoor Environment. *Journal of the Faculty of Agriculture*, Kyushu Univ., 56 (1), 139–148, 2011.

[8] Castenmiller C.J.J. Surface temperature of wooden window frames under influence of solar radiation. HERON, Vol. 49, No. 4, 2004.

[9] Karafil A., Ozbay H., Kesler M. and Parmaksiz H. Calculation of optimum fixed tilt angle of PV panels depending on solar angles and comparison of the results with experimental study conducted in summer in Bilecik, Turkey. *2015 9th International Conference on Electrical and Electronics Engineering (ELECO)*, Bursa, Turkey, 2015, pp. 971-976, doi: 10.1109/ELECO.2015.7394517.

[10] Tikkurila Valtti color safety data sheet. Available online: https://tikkurila.com/sites/default/files/valtti-color-sds-en.pdf (accessed on 10 March 2023).

[11] Fortino S, Hradil P. Metelli G. Moisture-induced stresses in large glulam beams. Case study: Vihantasalmi Bridge. *Wood Materials Science and Engineering* 14, 366-380, 2019.

[12] Brischke C., Alfredsen G., Humar M. Conti E., Cookson L., Emmerich L., Flæte P.O., Fortino S., Francis L., Hundhausen U. et al. Modeling the Material Resistance of Wood—Part 2: Validation and Optimization of the Meyer-Veltrup Model. *Forests* 12, 576, 2021.